

Multi-objective Optimization of a CNT/Polymer Nanocomposite Automotive Drive Shaft

M. H. Shojaeefard*¹, A. Khalkhali*² and Sh. Khakshournia*³

*1, 2 School of Automotive Engineering, Iran University of Science and Technology, Tehran, IRAN
mhshf@iust.ac.ir, ab_khalkhali@iust.ac.ir

*3 Ph. D student in School of Automotive Engineering, Iran University of Science and Technology
Technology, Tehran, IRAN
khakshournia@auto.iust.ac.ir

Abstract

Recent advances in ultra-small engineering sciences within two last decades have led scientists to produce new composite materials with Nano-dimensional fillers. Carbon nanotubes are samples of these materials. CNT/Polymer nanocomposites have vast application in industry because of their light weight and high strength. Predicting the properties of these materials and modeling them in simulation software products such as ABAQUS, makes it possible for us to reduce expenses of designing the parts composed of these materials. In this paper, a novel computational hybrid method is employed to calculate the mechanical properties of these materials. Using this method, analysis of automotive functionally graded nanocomposite drive shaft is carried out easily. Results of these analyses have shown that the distribution pattern of CNTs in the polymer matrix has great effect on final behavior and properties of the shaft. Finally, multi-objective optimization of the automotive drive shaft is carried out using NSGAI algorithm and a comparison is performed on weight, critical buckling torque and first fundamental torsion frequency of the current shaft and a similar composite shaft.

Keywords: automotive drive shaft, nanocomposite, carbon nanotube, RVE, functionally graded materials, multi-objective optimization, NSGAI

1 Introduction

Severe competition for producing more effective and simultaneously more economical productions, has made companies use novel materials instead of the old and classic ones. One of these prevalent novel materials is carbon nanotube (CNT). Carbon nanotubes have significant mechanical and electrical properties owing to their weird high ratio of length to diameter [1, 2 and 3].

It has been shown that it is possible to reach the same mechanical properties which we expect by addition of a certain value of micro-scaled reinforcer materials, if we add a remarkable less value of carbon nanotubes to the same polymer matrix [4, 5]. In 2004, Liu and Chen developed the presented model for composite materials reinforced by fiber, from Micro to Nano-scale and calculated the effective mechanical properties of composite materials reinforced by carbon nanotubes (CNTs) using a 3D Nano-scale element based on theory of elasticity and solving the finite element model [6]. A representative volume element (RVE) is made of one or

more Nano-filler(s) and constitutive matrix material which the required boundary conditions are applied on it to consider surroundings effects. In 2010, Hernandez-Perez et al [7] added an interphase layer to the former model, which is considered to model the atomic bonds effect in a CNT reinforced nanocomposite. They simulated the interphase modulus as a spatial function (gradient) between the modulus of CNT and matrix, to examine the influence of a linear and exponential gradient. Also several interphase thicknesses were examined. Finally, they found that an exponential function is more suitable than a linear one to represent the gradient of elastic properties occurring at the CNT-to-matrix interphase. Also they suggested that the interphase thickness must be at least of the order of the CNT thickness.

Functionally graded materials (FGMs) are novel composite materials which their microstructural details are spatially varied through non-uniform distribution of the reinforcement phase [8, 9]. Carbon nanotube reinforced composites (CNTRC) with functionally distribution of carbon nanotubes are widely studied in the recent years. For instance Hui Shen Shen et al [8] analyzed thermal buckling and post-buckling behavior of these composite materials. They showed that the buckling temperature as well as thermal post-buckling strength of the plate can be increased as a result of functionally graded reinforcement.

Distribution pattern of carbon nanotubes in the base polymer matrix, is clearly effective on the mechanical properties of final composite material. In a comparison of four different linear distribution patterns of carbon nanotubes by Ping Zhu et al. [10], it was concluded that if functionalization takes place as an X-formed pattern, the central deflection of carbon nanotube reinforced composite (CNTRC) plate will be minimum and the natural frequencies are more than the corresponding values for other linear patterns of distribution. It is clear that the difference in static and vibration responses originates from the difference in mechanical properties which is originated from the difference in patterns of functionalization [11, 12].

Drive shafts which are used to transmit the power, have diverse applications in the industry. A drive shaft is the main part of a power transmission system of an automotive. The length of automotive drive shafts are

usually limited by their critical speed. The critical speed of a drive shaft has inverse proportion with the square of that's length. The higher the fundamental natural torsion frequency of the shaft, the higher critical speed of that is [13]. Replacing the conventional metals with new high tech composite and nanocomposite materials as the constitutive material of a drive shaft, helps us to have lighter and longer drive shafts for a special critical speed. In the recent years, many studies are performed on composite and hybrid shafts. For instance, Li et al [14] performed designing and producing a hybrid Aluminum-Composite automotive drive shaft. They succeed to produce a drive shaft which was 75% lighter and 160% stronger than a metal drive shaft.

In this paper, initially a new computational method is developed to model the mechanical properties of functionally graded polymer/CNT nanocomposite with arbitrary distribution patterns and volume fractions of CNTs. This method is based on a coupling between two commercial software products, MATLAB and ABAQUS. Then, this method is employed to model drive shafts with different patterns of distribution and different volume fractions of CNTs. A comparison is carried out between these cases and interesting results are found. Subsequently, a multi-objective optimization is performed using modified-NSGAI algorithm considering weight, Critical buckling load and first torsional natural frequency as the conflicting objective functions of this optimization. This optimization has provided a set of non-dominant optimum design points. Finally, Nearest to Ideal Point (NIP) method is used to choose a compromising trade-off design point through the Pareto proposing points.

2 Effective elastic properties estimation

The RVE model proposed by Hernandez- Perez et al [7] is used in this paper to estimate the Young's modulus and Shear modulus and Poisson's ratios along the longitudinal and transverse directions. The RVE includes three phases, the matrix, the filler and the interphase which is a virtual material that is considered to model the atomic bonds between the matrix and filler atoms. The RVE is considered as a cylindrical tube. The model is created in commercial FEM software, ABAQUS. Three different loadings are applied to the RVE, as depicted in **Figure 1**; I- Tension II- Pressure III- Torsion. Small values of torque and stresses are applied as load in three mentioned cases to ensure that the deflections are in the elastic region. These values are considered as follows:

$$\sigma_0 = 1 \text{ nPa} \quad (1)$$

$$P_0 = 1 \text{ nPa} \quad (2)$$

$$T_0 = 10^{-17} \text{ N.m} \quad (3)$$

where, σ_0 , P_0 and T_0 are shown in **Figure 1**. The following values are about to be find in the three explained simulations:

(a) ΔL and ΔR_I , the RVE's length and radius variation

(b) ΔR_{II} , the RVE's radius variation

(c) α , the RVE's twist angle

Then, substitution of these values and (1) to (3) equations in the following equations leads to find the elastic

modulus and Poisson's ratios.

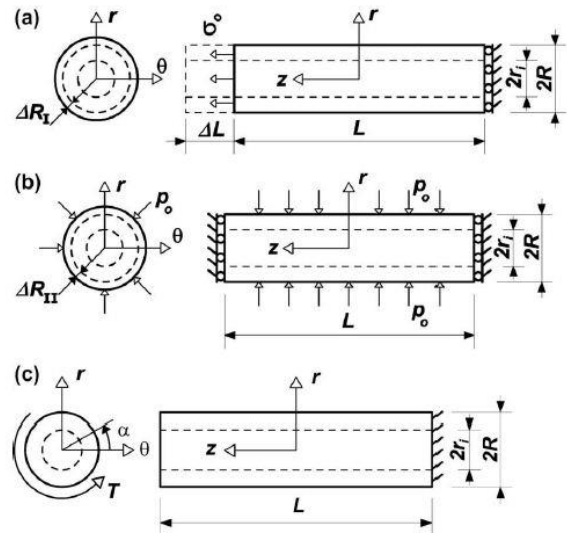


Figure 1 Different loading cases applied to the RVE- (a) Axial tension (b) Pressure (c) Torsion [7].

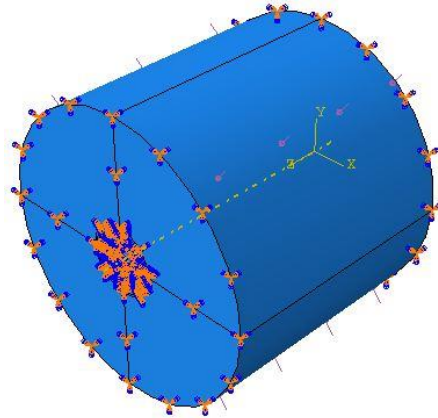


Figure 2 The RVE modeled in ABAQUS under pressure p_0 (Loading case. II).

$$E_z = \left(\frac{L}{\Delta L}\right)\sigma_z \quad (4)$$

$$\nu_{rz} = -\left(\frac{\Delta R_I}{R}\right)/\left(\frac{\Delta L}{L}\right) \quad (5)$$

$$G_{r\theta} = \frac{TL}{\alpha J} \quad (6)$$

$$E_r = \frac{4p_0R^2E_zG_{r\theta}}{p_0E_z(R^2-r_i^2)-2E_zG_{r\theta}\left(\frac{\Delta R_{II}}{R}\right)(R^2-r_i^2)+4p_0R^2\nu_{rz}^2G_{r\theta}} \quad (7)$$

$$\nu_{r\theta} = E_r \left[-\frac{\nu_{rz}^2}{E_z} + \frac{\Delta R_{II}}{Rp_0} + \left(-\frac{\nu_{rz}}{E_z} + \frac{1}{E_r} \right) \left(\frac{R^2+r_i^2}{R^2-r_i^2} \right) \right] \quad (8)$$

where, E_z and E_r are the Young's modulus along longitudinal and radius directions respectively, ν_{rz} and $\nu_{r\theta}$ are the Poisson's ratios, $G_{r\theta}$ is the shear modulus, L is length of the RVE, R and r_i are outer and inner radiuses of the RVE respectively and J is the polar moment of inertia of the RVE's section. Thickness of the interphase is considered as CNT's thickness. Two functions, linear and exponential are supposed to model the Young's modulus gradient in the interphase. Mechanical and geometrical properties of the CNT and the Matrix are considered as in [7] to provide possibility of making a comparison between the present model and the model presented in [7] in order to verify the present model. In the next sections of this paper, this RVE model

is used to simulate and analysis of a CNT/polymer automotive drive shaft. The polymer matrix's Young modulus varies from 1 to 100 *GPa*. The values of $E_z, E_r, G_{r\theta}, v_{rz}$ and $v_{r\theta}$ are calculated as different values of the Young modulus of matrix. **Figure 3** shows the variations of E_z and E_r with the matrix's Young modulus. Also the corresponding values found by [7] are compared with the present results and a good accordance is observed. E_m and E_t represent the Young modulus of matrix and CNT respectively. An exponential gradient is a better estimation for the interphase's modulus [7].

Figure 3 demonstrates that as E_m increases, the difference between exponential and linear gradient estimations decreases. Hence, the exponential gradient estimation for Young modulus of the interphase is remarkably better than a linear estimation in the case of modeling the polymer/CNT nanocomposites which the polymer matrix's Young modulus is a small value.

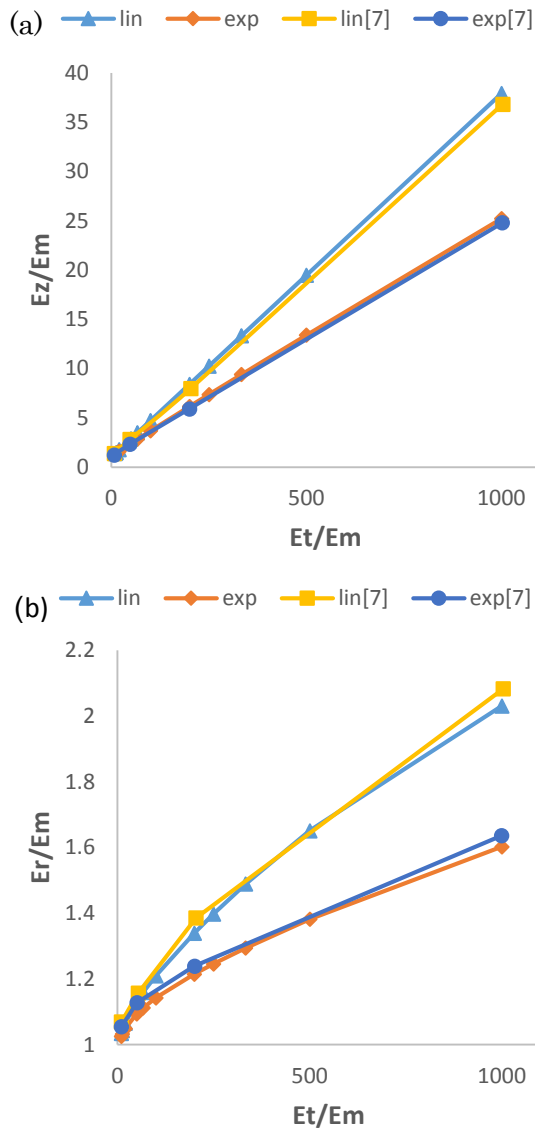


Figure 3 Effective composite properties as a function of E_t/E_m ($E_t = 1$ TPa), using linear and exponential gradient for the interphase modulus (a) Axial modulus, (b) Radial modulus.

3 Material configuration

The quality of CNTs' distribution in the matrix material may have a remarkable effect on final mechanical behavior of the nanocomposite drive shaft. This presumption is investigated further, by applying four different distribution patterns to the material; a uniform (UD) and three non-uniform distribution patterns (FG- Λ , FG-V and FG-X) are considered. **Figure 4** shows the quality of distribution for these patterns through the thickness of the drive shaft, where r_i and r_o are the inner and outer radii and V_{CNT}^* is the average volume percent of CNT in the nanocomposite.

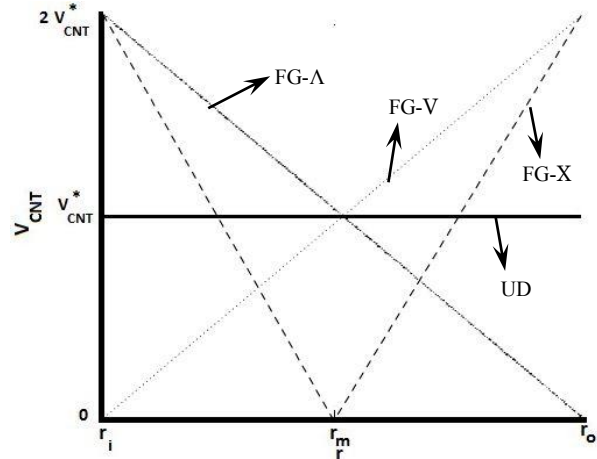


Figure 4 Volume fraction of CNT for different functionally graded distribution patterns as a function of radius.

The volume fraction of CNT for each distribution pattern is calculated using the following equations:

$$FG - V: V_{CNT} = 2 \left(\frac{r-r_i}{r_o-r_i} \right) V_{CNT}^* \quad (9)$$

$$FG - \Lambda: V_{CNT} = 2 \left(\frac{r_o-r}{r_o-r_i} \right) V_{CNT}^* \quad (10)$$

$$FG - X: V_{CNT} = 4 \left| \frac{r-r_m}{r_o-r_i} \right| V_{CNT}^*, \quad r_m = \frac{r_i+r_o}{2} \quad (11)$$

$$UD: V_{CNT} = V_{CNT}^* \quad (12)$$

4 FEM simulation of the drive shaft

The finite element modeling of the automotive drive shaft is performed using the commercial software, ABAQUS. The shaft is considered as a cylindrical tube with length of 1.73m and average diameter of 50.3mm. Constitutive matrix material of the nanocomposite is PmPV polymer with $E = 2.1$ GPa, $\rho = 1150$ kg/m³ and $\nu = 0.34$ [15]. Furthermore, the filler phase is considered as carbon nanotube with $E = 1$ TPa, $\rho = 1400$ kg/m³ and $\nu = 0.3$. S4R which is an element with 4 nodes and 6 DOF for each node is chosen as the element type. This element is typically used in shell analyses. **Figure 5** shows the FE model of the automotive drive shaft.

4.1 Torsional stiffness

In this analysis, the shaft is considered as a cantilever beam, which a 1 *KN.m* torque is applied to one end of it. The parametric study is performed on this shaft with varying the average CNT volume fraction (V_{CNT}^*) from

20% to 30%. Also, four distribution patterns which were explained in section 3 are applied to the shaft and the results are compared together. **Figure 6** shows the results of this analysis and comparison.

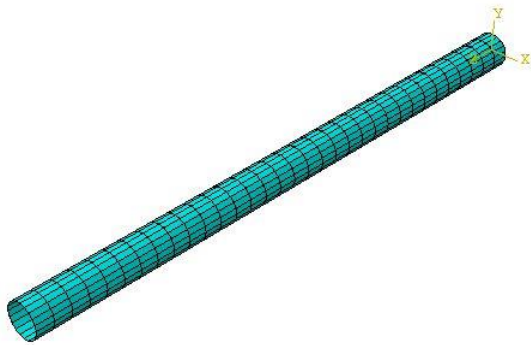


Figure 5 Finite element model of the nanocomposite automotive drive shaft.

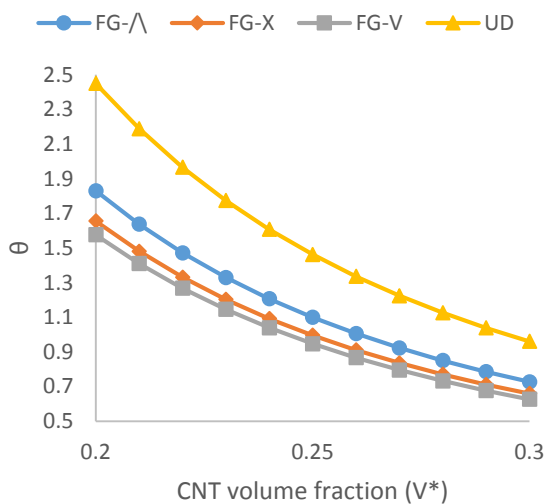


Figure 6 Twist angle of the drive shaft under 1 KN.m torque as a function of average CNT volume fraction for four different distribution patterns of CNTs.

Figure 6 shows that the twist angle of shaft's free end, is maximum for UD case and minimum for FG-V case. As a comparison, if $V^*=0.2$, the twist angle in UD case will be 1.55 times higher than the twist angle in FG-V case. Also, it is obvious that the lower volume fraction of CNTs, the higher difference between results of diverse distribution patterns of CNTs.

4.2 Modal analysis

The critical speed of an automotive drive shaft, limits by its first natural torsion frequency. The critical rotational speed of the shaft is 60 times higher than its fundamental torsion frequency. Hence, it is desired to higher fundamental torsion frequency of shaft. In this analysis, the shaft is considered as a cantilever beam and modeled in ABAQUS software. Then a modal analysis is performed on this shaft with varying the average CNT volume fraction (V_{CNT}^*) from 20% to 30%. Also, four distribution patterns which were explained in section 3 are applied to the shaft and the results are compared

together. **Figure 7** shows the results of this analysis and comparison.

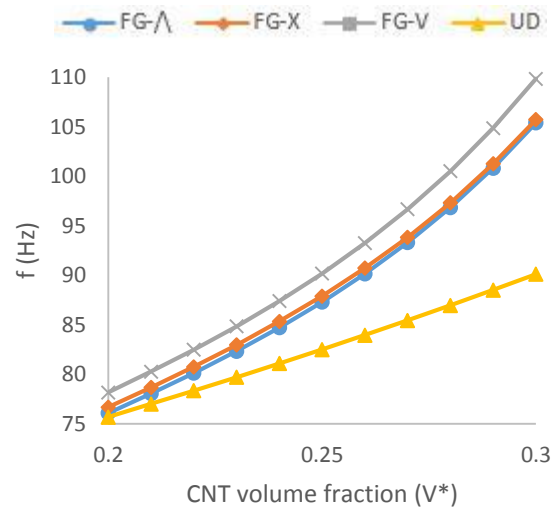


Figure 7 Fundamental torsion frequency of the drive shaft as a function of average CNT volume fraction for four different distribution patterns of CNTs.

Figure 7 shows that the fundamental torsion frequency of the shaft, is minimum for UD case and maximum for FG-V case. As a comparison, if $V^*=0.3$, the fundamental torsion frequency in FG-V case will be 1.23 times higher than the fundamental torsion frequency in UD case. Also, it is obvious that the higher volume fraction of CNTs, the higher difference between results of diverse distribution patterns of CNTs.

4.3 Critical buckling torque

The critical buckling torque is a limit that if the torque which is applied to the shaft reaches to this value, the shaft will lose its stability. The rotational buckling analysis for the automotive nanocomposite drive shaft is performed using ABAQUS software in this study. For this purpose, the shaft is modeled as a cantilever beam which a 1N.m torque is imposed to its free end with varying the average CNT volume fraction (V_{CNT}^*) from 20% to 30%. Also, four distribution patterns which were explained in section 3 are applied to the shaft and the results are compared together. **Figure 8** shows the results of this analysis and comparison.

Figure 8 shows that the critical buckling torque of the shaft, is minimum for FG-X case and maximum for FG-V case. As a comparison, if $V^*=0.3$, the critical buckling torque in FG-V case will be 1.2 and 2.14 times higher than the corresponding value in UD and FG-X cases respectively. Also, it is obvious that the higher volume fraction of CNTs, the higher difference between results of diverse distribution patterns of CNTs.

Now, it can be concluded that quality of distribution of CNTs through the matrix is remarkably effective on the final mechanical behavior of the automotive drive shaft. This is possible to effectively increase torsional stiffness, critical rotational speed and critical buckling torque of the nanocomposite automotive drive shaft, without consumption of more CNTs only by using a special distribution pattern of CNTs (FG-V). This fact leads to a simultaneous reduction in the shaft's weight.

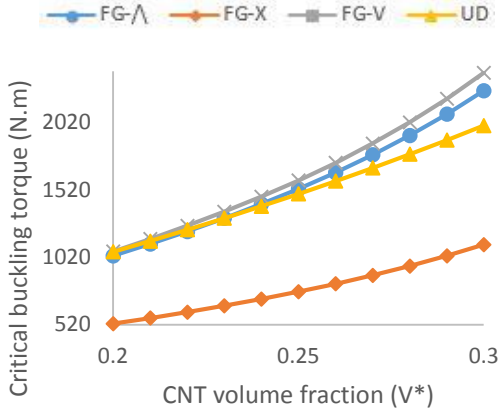


Figure 8 Critical buckling torque of the drive shaft as a function of average CNT volume fraction for four different distribution patterns of CNTs.

5 Multi-objective optimization

In multi-objective optimization we are looking for the design vector of $X^* = \{x_1^*, x_2^*, \dots, x_n^*\}^T$ element R^n which optimizes the objective functions $F = \{f_1(X), f_2(X), \dots, f_k(X)\}^T$ element R^k under m unequal constraints:

$$g_i(X) \leq 0 \quad i=1, 2, \dots, m \quad (13)$$

And p equal constraints

$$h_j(X) = 0 \quad j=1, 2, \dots, p \quad (14)$$

Without reducing generality of the problem, we suppose that all objective vectors should be minimized. This multi-objective minimization problem that is categorized as Pareto problems is defined as follows.

Pareto dominance:

Vector $U = [u_1, u_2, \dots, u_n]$ is dominated to vector $V = [v_1, v_2, \dots, v_n]$ where $(U < V)$, if and only if:

$$\forall i \in \{1, 2, \dots, k\}, u_i \leq v_i \wedge \exists j \in \{1, 2, \dots, k\}, u_j < v_j. \quad (15)$$

Pareto optimality:

A point such as $X^* \in \Omega$ (Ω is an acceptable design region which satisfies the equations (13) and (14)) is an optimum Pareto if and only if $F(X^*) < F(X)$. Or in other words:

$$\forall i \in \{1, 2, \dots, k\}, \forall X \in \Omega - \{X^*\}, f_i(X^*) \leq f_i(X) \wedge \exists j \in \{1, 2, \dots, k\} : f_j(X^*) < f_j(X) \quad (16)$$

Pareto set:

In multi-objective optimization problem, a Pareto set (P^*) contains all optimized Pareto vectors:

$$P^* = \{X \in \Omega | \exists X \in \Omega : F(X') < F(X)\}. \quad (17)$$

In this paper, we used modified NSGA-II algorithm which is usable for the optimization problem with infinite objective functions.

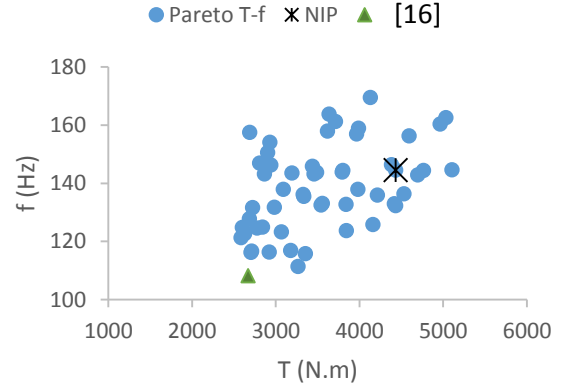


Figure 9 Pareto front of fundamental torsion frequency and critical buckling torque.

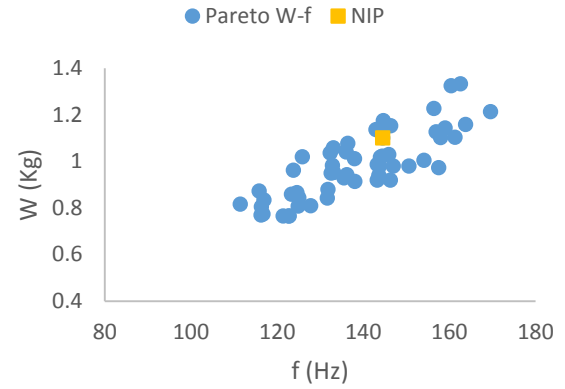


Figure 10 Pareto front of weight and fundamental torsion frequency.

To achieve an optimum design for the automotive drive shaft, a multi-objective optimization problem considering three conflicting objective functions (average volume fraction of CNTs (V_{CNT}^*), the shafts thickness (t) and average radius of the shaft (r_m)) is solved using NSGAI algorithm. The finite element model described in section 4 and the NSGAI algorithm are employed simultaneously in this study using a coupling between two commercial software products, ABAQUS and MATLAB. The optimization problem could be summarized as:

$$\left\{ \begin{array}{l} \text{Minimize } f_1 = W(V_{CNT}^*, r_m, t) = \\ (\rho_m V_m + \rho_{CNT} V_{CNT}^*) \times \left(\pi L \left(\left(r_m + \frac{t}{2} \right)^2 - \left(r_m - \frac{t}{2} \right)^2 \right) \right) \\ \text{Maximize } f_2 = f(V_{CNT}^*, r_m, t) \\ \text{Calculated using ABAQUS PYTHON code} \\ \text{Maximize } f_3 = T(V_{CNT}^*, r_m, t) \\ \text{Calculated using ABAQUS PYTHON code} \\ \text{Under constraints: } W < 3 \text{ kg} \\ T >= 2030 \text{ N.m} \\ f > 90.5 \text{ Hz} \\ \text{Design variables' interval:} \\ V_{CNT}^*: [0.15, 0.32] \\ r_m: [0.015, 0.035] \\ t: [0.0005, 0.003] \end{array} \right. \quad (18)$$

The Pareto fronts obtained by the optimization process is shown in **Figures 9-10**. Results are compared with the results found by [19] which is a similar optimization on a composite automotive drive shaft.

The trade-off optimum design point, which is the best compromising design point introduced by NIP (Nearest to Ideal Point method) is figured out and shown on **Figures 9 and 10**. As it is obvious on **Figures 9**, the Pareto non-dominant optimum design points are placed in the right and top side of the trade-off optimum point reported by [19] for the automotive composite drive shaft. This fact shows that a CNT/Polymer nanocomposite drive shaft will have a higher critical buckling torque and simultaneously a higher critical rotational speed in comparison with a similar composite drive shaft. **Table 1** makes it possible to compare the present work's results with reported results of [19]. All three objective functions are reduced in comparison with corresponding results for a composite automotive drive shaft.

Table 1 Trade-off design points comparison

	f (Hz)	W (Kg)	Tcr (KN.m)
NIP	144.51	1.100	4433.5
[19]	108.33	2.87	2670

6 Conclusion

In this paper, a new method was employed to model the effective properties of a functionally graded nanocomposite by using a coupling between ANSYS and ABAQUS software products. Subsequently, a multi-objective optimization was performed on a nanocomposite automotive drive shaft, with the purpose of minimizing the weight and maximizing the fundamental torsion frequency and the critical buckling torque. This optimization was carried out using a coupling between the commercial software products, ABAQUS and MATLAB. The results of optimization including a set of non-dominant optimum design points was reported. Designers are free to choose one of these points related to their preferences. Then, a compromising trade-off point was introduced using NIP method. A comparison between the results of present study and a similar composite automotive drive shaft in **Figure 9** and **Table 1**, showed that using a CNT/PmPV nanocomposite drive shaft with a particular distribution pattern of CNTs (FG-V) instead of a composite or aluminum one, will lead to a remarkable improvement in mechanical properties of the shaft.

References

[1] Wang X., Qunqing L., Xie J., Jin Z.; Wang J., Li Y., Jiang K.; Fan S., "Fabrication of ultralong and electrically uniform single-walled carbon nanotubes on clean substrates", *Nano Lett.* Vol. 9, (2009), pp. 3137-41.
 [2] Coleman JN., Khan U., Blau WJ., Gun'ko YK., "Small but strong: A review of the mechanical properties of carbon nanotube-polymer composites." *Carbon* Vol. 44, (2006), pp. 1624-52.
 [3] Fielder B., Gojny FH., Wichmann MHG., Nottle MCM., Schulte K., "Fundamental aspects of nano-reinforced composites", *Compos Sci Technol*, Vol. 66, (2006), pp. 3115-25.

[4] Thotenson ET.; Ren Z., Chou T-W., "Advances in science and technology of carbon nanotubes and their composites: a review", *Compos Sci technol.* Vol. 61, (2001), pp. 1899-912.
 [5] Barber AH., Cohen SR., Wanger HD., "Measurement of carbon nanotube-polymer interfacial strength." *Appl Phys Lett.*, Vol. 82, (2003), pp. 4140-2;
 [6] X. Chen and Y. J. Liu, "Square representative volume elements for evaluating the effective material properties of carbon nanotube-based composites." *Computational Material Science*, Vol. 29, (2004), pp. 1-11.
 [7] A. Hernandez-Perez, F. Aviles, "Modeling the influence of interphase on elastic properties of carbon nanotube composites", *Computational Materials Science*, Vol. 47, (2010), pp. 926-33.
 [8] Shen H.S., Zhang C.L., "Thermal buckling and postbuckling behavior of functionally graded carbon nanotube-reinforced composite plates", *Mater Des.*, Vol. 31, (2010), pp. 3403-11.
 [9] Ma P-C., Mo S-Y., Tang B-Z., Kim J-K., "Dispersion, interfacial interaction and re-agglomeration of functionalized carbon nanotubes in epoxy composites.", *Carbon.*, Vol. 48, pp. 1824-34.
 [10] Zhu P., Lei Z.X., Liew K.M., "Static and free vibration analysis of carbon nanotube-reinforced composite plates using finite element method with first order shear deformation plate theory", *Compos struc.*, Vol. 94, (2012), pp. 1450-60.
 [11] Ke L-L., Yang J., Kitipornchai S., "Nonlinear free vibration of functionally graded carbon nanotube-reinforced composite beams". *Compos Struct.*, Vol. 92, (2010), pp. 676-83.
 [12] Shen HS., Zhu ZH., "Buckling and postbuckling behavior of functionally graded nanotube-reinforced composite plates in thermal environments." *CMC Comput Mat Contin.* Vol. 18, (2010), pp. 155-82.
 [13] F. Schmelz, Seherr-Thoss, E. Aucktor, "Universal joints and drive shaft", Springer-Verlag, New York, (1992).
 [14] D.G. Lee, Hak Sung Kim, Jong Woon Kim, Jin Kook Kim, "Design and manufacture of an automotive hybrid aluminum/composite drive shaft" , *Composite Structures*, Vol. 63, (2004), pp. 87-99.
 [15] Han Y, Elliott J. , "Molecular dynamics simulations of the elastic properties of polymer/carbon nanotube composites.", *Comput Mater Sci*, Vol. 39, (2007), pp. 315-23.
 [16] E. Nikghalb, "Optimum design of a composite automotive drive shaft", Final thesis of B. SC's degree, IUST University, (2013).

Received on October 31, 2013
 Accepted on January 23, 2014